Quinone (Q B) Binding Site and Protein Stuctural Changes in Photosynthetic Reaction Center Mutants at Pro-L209 Revealed by Vibrational Spectroscopy

4 **AUTHORS**, INCLUDING:

Pierre Sebban
Université Paris-Sud 11
77 PUBLICATIONS **1,532** CITATIONS

SEE PROFILE

Laura Baciou
French National Centre for Scientific Research
44 PUBLICATIONS **893** CITATIONS

SEE PROFILE

Quinone (Q$_B$) Binding Site and Protein Stuctural Changes in Photosynthetic Reaction Center Mutants at Pro-L209 Revealed by Vibrational Spectroscopy

Eliane Nabedryk,*,‡ Jacques Breton,‡ Pierre Sebban,§ and Laura Baciou§

Service de Bioénergétique, CEA-Saclay, 91191 Gif-sur-Yvette Cedex, France, and Centre de Génétique Moléculaire, CNRS, 91198 Gif-sur-Yvette, France

ABSTRACT: The effect of substituting Pro-L209 with Tyr, Phe, Glu, and Thr in photosynthetic reaction centers (RCs) from *Rhodobacter sphaeroides* was investigated by monitoring the light-induced FTIR absorption changes associated with the photoreduction of the secondary quinone Q$_B$. Pro-L209 is close to a chain of ordered water molecules connecting Q$_B$ to the bulk phase. In wild-type RCs, two distinct main Q$_B$ binding sites (distal and proximal to the non-heme iron) have been described in the literature. The X-ray structures of the mutant RCs Pro-L209 → Tyr, Pro-L209 → Phe, and Pro-L209 → Glu have revealed that Q$_B$ occupies a proximal, intermediate, and distal position, respectively [Kuglstatter, A., Ermler, U., Michel, H., Baciou, L., and Fritzsch, G. (2001) *Biochemistry 40*, 4253−4260]. FTIR absorption changes associated with the reduction of Q$_B$ in Pro-L209 → Phe RCs reconstituted with ^{13}C-labeled ubiquinone show a highly specific IR fingerprint for the C=O and C=C modes of Q$_B$ upon selective labeling at C$_1$ or C$_4$. This IR fingerprint is similar to those of wild-type RCs and the Pro-L209 → Tyr mutant [Breton, J., Boullais, C., Mioskowski, C., Sebban, P., Baciou, L., and Nabedryk, E. (2002) *Biochemistry 41*, 12921−12927], demonstrating that equivalent interactions occur between neutral Q$_B$ and the protein in wild-type and mutant RCs. It is concluded that in all RCs, neutral Q$_B$ in its functional state occupies a unique binding site which is favored to be the proximal site. This result contrasts with the multiple Q$_B$ binding sites found in crystal structures. With respect to wild-type RCs, the largest FTIR spectral changes upon Q$_B$$^-$ formation are observed for the Phe-L209 and Tyr-L209 mutants which undergo similar protein structural changes and perturbations of the semiquinone modes. Smaller changes are observed for the Glu-L209 mutant, while the vibrational properties of the Thr-L209 mutant are essentially the same as those for native RCs.

The reaction center (RC)[1] from the photosynthetic purple bacterium *Rhodobacter* (*Rb.*) *sphaeroides* is a transmembrane protein complex that couples the light-induced transfer of two electrons and two protons to the secondary quinone Q$_B$ to form the quinol which then leaves the RC to be oxidized by another membrane protein complex, the cytochrome *bc*$_1$ complex (*1*). The resulting transmembrane proton gradient drives ATP synthesis. Since Q$_B$ is located in the interior of the protein, the protons required to stabilize the reduced quinone must be conducted through the protein from the cytoplasmic surface to the Q$_B$ binding site. In the high-resolution structures of bacterial RCs, chains of protonatable amino acid residues and ordered water molecules that connect Q$_B$ to the bulk phase have been identified (*2–6*) and are presumably used for the uptake, transport, and delivery of protons to Q$_B$. A number of spectroscopic studies of site-directed mutant RCs from *Rb. sphaeroides* (for reviews, see refs *1*, *7*, and *8*) have led to the identification of specific ionizable side chains, such as the key residues Glu-L212, Asp-L213, Ser-L223, Asp-M17, Asp-L210, and Glu-H173, that are likely to be involved in the proton pathway to Q$_B$. Several of these residues are potentially connected to bound water molecules. However, the question of a unique entry point for the proton (*9–11*) or different protonation pathways (*12, 13*) is still under debate. It has been shown that the first electron-transfer step from Q$_A$$^-$ to Q$_B$ with rate $k_{AB}(1)$, which does not involve direct protonation of the quinone, is coupled to the protonation of Glu-L212 (*14–18*), and that the change of the ionization state of this carboxylic acid is the main response of the carboxylic cluster located near Q$_B$ upon Q$_B$$^-$ formation (*14, 19–21*). The second electron-transfer step is coupled to direct protonation of the quinone, and the proton pathway for the two protons to reduced Q$_B$ is proposed to involve several carboxylic acids before branching to Glu-L212 (*17*). In this study, we will focus on the first electron transfer to Q$_B$.

Besides mutations of protonatable residues near Q$_B$ that can affect the electrostatic environment and thus the electron/proton-transfer rates, point mutations at the rigid Pro-L209 side chain (*22*) were originally designed to interrupt a water chain connecting Q$_B$ to the bulk phase. Pro-L209 is located 9 Å from Q$_B$ and is close to two water molecules belonging to a chain of 12 ordered water molecules. Mutations have

---

* Corresponding author: Eliane Nabedryk, SBE, CEA-Saclay, Bât. 532, 91191 Gif-sur-Yvette Cedex, France. Phone: 331 69 08 71 12. Fax: 331 69 08 87 17. E-mail: nabedryk@dsvidf.cea.fr.
‡ Service de Bioénergétique, CEA-Saclay.
§ Centre de Génétique Moléculaire, CNRS.
[1] Abbreviations: RC, reaction center; WT, wild-type; Q$_A$, Q$_B$, primary, secondary quinone electron acceptor; Q$_n$, 2,3-dimethoxy-5-methyl-6-polyprenyl-1,4-benzoquinone; FTIR, Fourier transform infrared spectroscopy.
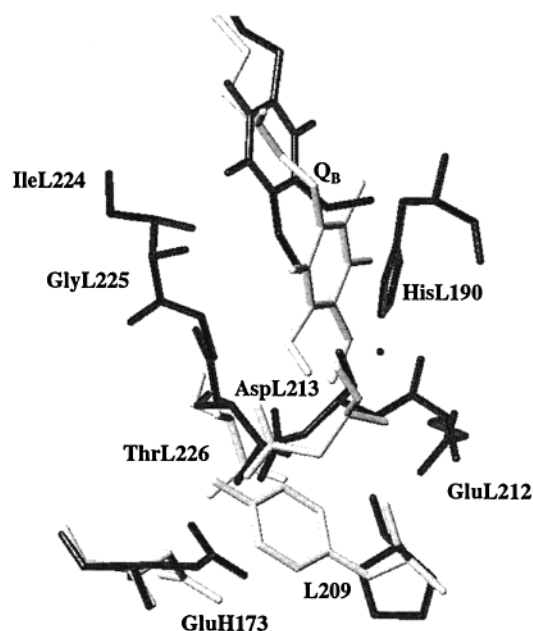
FIGURE 1: Comparison of the Q_B binding pocket in the X-ray structures of wild-type RC from *Rb. Sphaeroides* (PDB entry 1PCR) drawn in black and the Pro-L209 → Tyr RC (PDB entry 1F6N) drawn in gray. Several side chain residues that are either ligands to the Q_B carbonyls or which position varies between the wild-type and mutant RCs are indicated.

involved aromatic (Tyr, Phe, Trp), carboxylic (Glu), and hydroxylic (Thr) side chains (*22*, *23*). In the aromatic mutants, the proton-coupled second transfer reaction and the proton uptake kinetics after the second flash are notably decreased compared to wild-type (WT) RCs (*23*). The mutations Pro-L209 → Phe and Pro-L209 → Trp also reduce the first electron-transfer rate. In the Thr- and Glu-L209 mutants, the kinetic parameters are similar to those of WT RCs. The alteration of the electron/proton-transfer properties in the aromatic mutants (*22*–*24*) suggests structural changes in the organization of the chain of protonatable residues and water molecules.

Recently, the structures of three mutant RCs at the L209 position have been determined by X-ray crystallography (*25*). The X-ray analysis reveals that the Pro-L209 → Tyr and Pro-L209 → Phe mutations do not interrupt the water chain while in the Pro-L209 → Glu mutant, the introduced Glu-L209 side chain replaces two water molecules. Moreover, the high-resolution structures of the Tyr-L209 (Figure 1) and Phe-L209 RCs show similar structural changes around Q_B, with significant displacements of several polar amino acid side chains (Asp-L213, Thr-L226, Glu-H173) by up to 2.6 Å, but no changes in the protein backbone (*25*). In contrast, no significant structural changes were observed in the Glu-L209 mutant. Interestingly, the mutations differently affect the position of Q_B in the Phe-, Tyr-, and Glu-L209 RCs.

In the crystals of WT RCs from *Rb. sphaeroides*, the Q_B molecule was found at two different main positions, proximal (*4*, *26*–*30*) and distal (*2*, *4*, *30*; see also Figure 1) to the non-heme iron. In the work of Stowell et al. (*4*) at 90 K, Q_B occupies a distal position in the dark-adapted crystals (refined to 2.2 Å) and a proximal position in the charge-separated state $P^+Q_B^-$ (at 2.6 Å resolution): Q_B^- is located ~5 Å from the Q_B distal position in the neutral PQ_B state. However, a partially occupied proximal binding site was likely in the

dark-adapted structure. In the more recent work of Fritzsch et al. (*30*) at −150 °C, the distal site has an occupancy of 55% and the proximal site of 45% in the dark state (at 1.87 Å resolution) with a ~4.5 Å distance between the two positions. In the light-excited state (at 2.07 Å resolution), the occupancies are 10 and 90%, respectively. In both structures of Stowell et al. (*4*) and Fritzsch et al. (*30*), the displacement of Q_B between the two positions is accompanied by a 180° ring flip and only one carbonyl of Q_B interacts with the protein (backbone NH of Ile-L224) in the distal site, while the two carbonyls form polar interactions with the surrounding protein in the proximal site, notably with His-L190 for the proximal $C_4{=}O^2$ of Q_B. The description of two binding sites for Q_B has provided a molecular basis for a conformational gating model limiting the rate of the first electron transfer from Q_A^- to Q_B (*31*, *32*), and has triggered a number of theoretical works on the functional implications of the two distinct Q_B positions (*33*–*38*). Some of these studies (*35*, *37*–*38*) as well as recent experimental work (*39*–*41*), however, suggest that Q_B movement is not the sole contribution to the conformational gating step.

In the dark-adapted crystals of Tyr-L209 RCs at 5 °C (*25*), only one site is described for the location of Q_B which is the proximal one (Figure 1). The position of Q_B in the Tyr-L209 mutant is thus similar to the one found for WT RCs after illumination at low temperature (*4*, *30*). However, the Q_B ring in the Tyr-L209 mutant does not seem to undergo a 180° twist around the isoprenoid tail compared to the ring orientation in the light-adapted structure of WT RCs. In the Phe-L209 mutant, the best fit for Q_B was obtained for an intermediate position of Q_B between the distal and proximal binding sites (*25*). In the aromatic mutants, the displacement of Q_B and the rearrangement of several side chains (Figure 1) could lead to a reorganization of the hydrogen-bonded networks close to Q_B. In contrast, no significant structural changes were observed in the Glu-L209 RC and a distal binding site was suggested for Q_B in this mutant (*25*).

Besides X-ray crystallography, the binding of quinones (Q_A and Q_B) in native and mutant RCs can be investigated in detail by vibrational spectroscopy (*42*). FTIR studies of RCs reconstituted with site-specific isotope labeled quinones have previously provided information on the bonding interactions of Q_B (and Q_A) in native RCs from *Rb. sphaeroides* and *Rhodopseudomonas* (*Rp.*) *viridis* (*42*, *43*–*45*), and in mutant RCs (*46*, *47*). Recently, a study of the FTIR vibrational properties of the neutral Q_B molecule in the Pro-L209 → Tyr mutant was performed (*47*). Light-induced absorption changes associated with the reduction of Q_B in the Pro-L209 → Tyr RCs reconstituted with $^{13}C_1$- or $^{13}C_4$-labeled Q_3^2 show a highly specific IR fingerprint for the C=O and C=C modes of Q_B (*47*), which is similar to that of WT RCs (*44*). In both native and mutant RCs, the two carbonyls of neutral Q_B absorb at 1641 ± 1 cm^{-1}, indicative of symmetric and moderate hydrogen bonding interactions with the protein. However, the different coupling of the C=O and C=C Q_B modes noticed for the C_1 and C_4

---

[2] For isolated Q_3, the C_1 and C_4 labels are on the C=O adjacent to the isoprene chain and the methyl group, respectively. In the proximal Q_B conformation, the C_1 and C_4 carbon atoms are on the distal and proximal sites, respectively.

atoms reflects some asymmetry in the specific anchoring of the quinone in its binding pocket (*44*). Since the FTIR data fit the description of the proximal site with the two carbonyls interacting with the protein, it was concluded that Q_B occupies the same binding site in native and Tyr-L209 RCs and that neutral Q_B in its functional state also binds to the proximal site in WT RCs (*47*).

In addition to the determination of the bonding interactions of the neutral Q_B, light-induced FTIR difference spectroscopy provides means to explore the protein structural rearrangements (backbone and side chains), the changes of protonation state of carboxylic acids, and the semiquinone–protein interactions (*14*, *42*, *44*, *45*). In this report, the effect of substituting Pro-L209 with Thr, Glu, Phe, and Tyr in RCs from *Rb. sphaeroides* was investigated by monitoring in ^1H_2O and ^2H_2O the light-induced FTIR absorption changes associated with the photoreduction of Q_B. Since Q_B occupies different positions in the X-ray structures of the L209 mutants, the vibrational properties of Q_B should differ for the Tyr-, Phe-, and Glu-L209 RCs. Interactions of Q_B and Q_B^- with the protein in the Phe-L209 mutant were investigated by using site-specific ^{13}C-labeled ubiquinone to reconstitute the Q_B site, and were compared to those previously found for the Tyr-L209 RCs (*47*). With respect to WT RCs, the largest FTIR spectral changes are observed for the two aromatic mutant RCs Phe-L209 and Tyr-L209 which undergo similar protein structural changes as well as similar perturbations of the semiquinone modes upon first electron transfer to Q_B. On the other hand, identical bonding interactions of the neutral Q_B with the protein are found in all native and mutant RCs and it will be shown that these data can be related to an identical Q_B position at the proximal site in functional RCs.

MATERIALS AND METHODS

The construction of the site-directed mutants and the isolation of purified RCs are described in ref *22*. A detailed description of the preparation of RC samples for FTIR experiments is given in refs *14* and *44*: RC samples (∼0.2 mM) in 90 mM Tris buffer (pH 7) contained an excess of ubiquinone (Q_6 or Q_3). Q_6 was purchased from Sigma. The synthesis of Q_3 selectively labeled with ^{13}C at the 1- or the 4-position has been reported previously (*48*). The preparation of RC samples in ^2H_2O was carried out as reported in ref *19*.

Steady-state light-induced FTIR difference spectra of the Q_B to Q_B^- transition in native and mutant RCs were recorded at 15 °C with a Nicolet 60SX spectrometer, as described in refs *14* and *44*. The Q_B^- state was generated by excitation with a single saturating flash (Nd:YAG laser, 7 ns, 530 nm). Difference spectra were calculated from each 128 scans (acquisition time: 23 s) recorded before and after laser flash excitation. For a given sample, these measurements were repeated over ∼30 h. Spectra are an average of two to three samples.

RESULTS

Q_B^-/Q_B Spectra of Wild-Type and Mutant (Pro-L209 → Thr, Glu, Phe, Tyr) RCs in ^1H_2O. Figure 2 shows the Q_B^-/Q_B light-induced FTIR difference spectra in ^1H_2O of WT and mutant (Pro-L209 → Thr, Glu, Phe, Tyr) RCs recon-
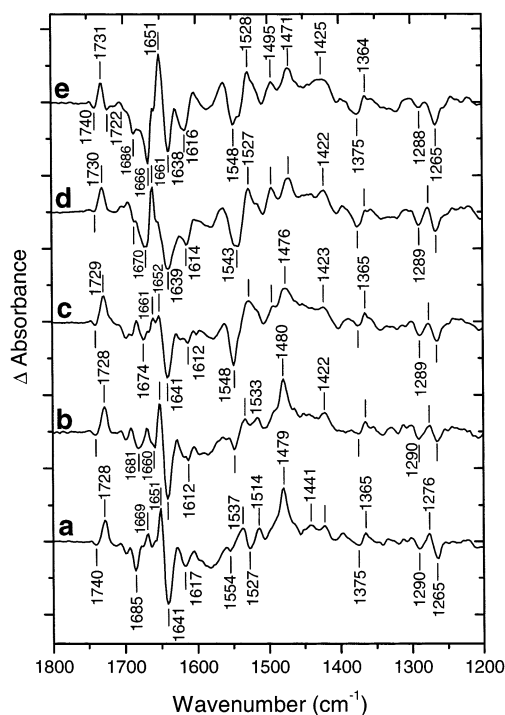

FIGURE 2: Light-induced Q_B^-/Q_B FTIR difference spectra in ^1H_2O at pH 7, 15 °C of wild-type (a) and mutant (b−e) RCs from *Rb. sphaeroides* reconstituted with unlabeled Q_6; (b) the Pro- L209 → Thr mutant; (c) the Pro-L209 → Glu mutant; (d) the Pro-L209 → Phe mutant; (e) the Pro-L209 → Tyr mutant. About 100 000 interferograms were averaged. The tick marks on the vertical axis are separated by 2.5×10^{-4} absorbance units. The frequency of the IR bands is given with an accuracy of ± 1 cm^{-1}. Spectral resolution was 4 cm^{-1}.

stituted with unlabeled Q_6. In WT RCs (Figure 2a), absorption changes associated with the first electron transfer to Q_B have been previously assigned to modes of the semiquinone (C⋯O and C⋯C at 1479 cm^{-1}), the neutral quinone (C=O at 1641 cm^{-1}, C=C at 1617 cm^{-1}, C−O−CH_3 at 1265 and 1290 cm^{-1}), and the protein at 1728, 1685, 1651, 1641, 1554, 1537, 1527, and 1514 cm^{-1} (*14*, *42*, *44*). Among the series of L209 mutants, the Q_B^-/Q_B spectrum of Thr-L209 RCs (Figure 2b) is the only one that is close to that of native RCs. Similarly to native RCs, it displays a main positive anion band at 1480 cm^{-1}, a differential signal at 1652/1641 cm^{-1} lying in the amide I (80% peptide C=O stretching; *49*) and in the Q_B C=O (at least partially at 1641 cm^{-1}) spectral ranges, and a positive band at 1728 cm^{-1}, which, in native RCs, has been assigned to protonation of Glu-L212 upon Q_B^- formation (*14*, *15*). A few signals are however affected in Thr-L209 RCs, notably at ∼1548 and 1533 cm^{-1} in the amide II region (60% peptide NH bending and 40% C−N stretching; *49*) and at 1681 cm^{-1}.

In contrast to the Thr-L209 RCs, the Q_B^-/Q_B spectra of the aromatic and carboxylic mutants display drastic differences in the whole 1750−1400 cm^{-1} region, although the general IR pattern of the two aromatic mutants is closely related. Both spectra of Phe-L209 (Figure 2d) and Tyr-L209 (Figure 2e) RCs show two bands at 1471 and 1495 cm^{-1} instead of the main semiquinone band at 1479 cm^{-1} in native RCs. They also show similar changes in the amide II region with a large negative signal at ∼1548−1543 cm^{-1} and a positive signal at 1528−1527 cm^{-1}. A differential signal is observed at 1651/1638 cm^{-1} (shoulder at 1661 cm^{-1}) in Tyr-
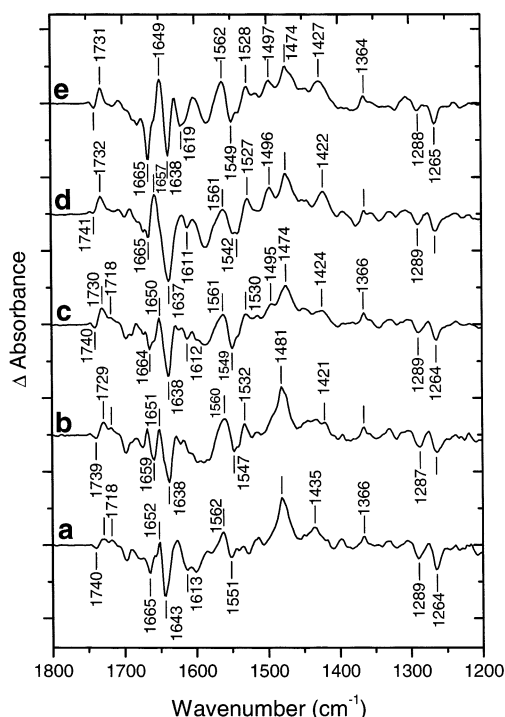
FIGURE 3: Light-induced Q_B^-/Q_B FTIR difference spectra in ^2H_2O at pH 7, 15 °C of wild-type (a) and mutant (b−e) RCs from *Rb. sphaeroides* reconstituted with unlabeled Q_6; (b) the Pro-L209 → Thr mutant; (c) the Pro-L209 → Glu mutant; (d) the Pro-L209 → Phe mutant; (e) the Pro-L209 → Tyr mutant. About 100 000 interferograms were averaged. The tick marks on the vertical axis are separated by 2.5×10^{-4} absorbance units.

L209 RCs, and at 1661/1639 cm^{-1} (shoulder at 1653 cm^{-1}) in Phe-L209 RCs, compared to the one seen at 1651/1641 cm^{-1} in native RCs. In addition, the two aromatic mutants display a new large negative signal at 1666 cm^{-1} (Tyr-L209) and 1670 cm^{-1} (Phe-L209).

The Q_B^-/Q_B spectrum of Glu-L209 RCs (Figure 2c) shows a main Q_B^- band at 1476 cm^{-1} with a shoulder at 1495 cm^{-1}, and small positive signals at 1661 and 1652 cm^{-1} instead of the large peak seen at 1651 cm^{-1} in WT RCs. Similarly to the two aromatic mutants, large changes are seen in the amide II region at 1548 and 1527 cm^{-1}.

In all the mutant spectra (Figure 2), contributions from the methoxy groups of Q_B are consistently detected at ∼1290 and 1265 cm^{-1}. Above 1700 cm^{-1}, the Q_B^-/Q_B spectra show a main positive band peaking at 1728 cm^{-1} for WT and Thr-L209 RCs, and at 1729, 1730, and 1731 cm^{-1} for Glu-, Phe-, and Tyr-L209 RCs, respectively. A small negative signal at 1740 cm^{-1} is consistently observed in all the spectra.

Q_B^-/Q_B Spectra of Native and Mutant (Pro-L209 → Thr, Glu, Phe, Tyr) RCs in ^2H_2O. In WT RCs, large effects of $^1H/^2H$ exchange have been previously observed (*14*, see also Figure 3a). The Q_B^-/Q_B spectra of the L209 mutant RCs were obtained in ^2H_2O (Figure 3b−e) to identify bands that are sensitive to deuterium exchange. Similarly to native RCs where a small isotopic effect occurs for the semiquinone band in ^2H_2O, the main Q_B^- peak in Thr-L209 RCs is upshifted from 1480 cm^{-1} in ^1H_2O (Figure 2b) to 1481 cm^{-1} in ^2H_2O (Figure 3b). For the aromatic mutants, the bands seen at 1471 and 1495 cm^{-1} in ^1H_2O (Figure 2d,e) are also upshifted in ^2H_2O by 3 and 1−2 cm^{-1}, respectively (Figure 3d,e). For

the Glu-L209 mutant, the 1476 cm^{-1} band in ^1H_2O (Figure 2c) peaks at 1474 cm^{-1} in ^2H_2O (Figure 3c).

In all native and mutant RCs, additional isotopic effects are observed in the 1630−1690 cm^{-1} spectral region where contributions from peptide C=O and side chains are expected (*49*). A frequency downshift by a few wavenumbers upon $^1H/^2H$ exchange (Figure 3) is observed for the main peaks seen in ^1H_2O (Figure 2) at 1652 (−1) and 1641 (−3) cm^{-1} in Thr-L209, at 1652 (−2) and 1641 (−3) cm^{-1} in Glu-L209, at 1670 (−5), 1661 (−4), and 1639 (−2) cm^{-1} in Phe-L209, and at 1666 (−1) and 1651 (−2) cm^{-1} in Tyr-L209. Also, the amplitude of the signals present in the amide II region at ∼1548/1528 cm^{-1} in ^1H_2O for the spectra of the carboxylic and aromatic mutants is consistently reduced in ^2H_2O, in agreement with $^1H/^2H$ exchange of peptide NH groups.

In the region between 1770 and 1700 cm^{-1}, signals arising from the C=O stretching vibrations of protonated Asp or Glu side chains are expected to be sensitive to $^1H/^2H$ exchange (*14*), while signals arising from the ester C=O modes of pigments will be little affected by deuterium exchange (*50*). In native RCs, the downshift of the band at 1728 cm^{-1} in ^1H_2O to ∼1718 cm^{-1} in ^2H_2O has been previously attributed to the $^1H/^2H$ effect on the C=O mode of the protonated side chain of Glu-L212 (*14, 19−21*). Similarly to native RCs, the amplitude of the positive band at 1728−1729 cm^{-1} in the Thr-L209 (Figure 2b) and Glu-L209 (Figure 2c) mutants is reduced in ^2H_2O and a new positive peak appears at ∼1718 cm^{-1} (Figure 3b,c). On the other hand, the spectra of the Phe-L209 (Figure 3d) and Tyr-L209 (Figure 3e) RCs in ^2H_2O show a band at 1731−1732 cm^{-1} which is broadened on its low energy side, with no apparent new positive feature. In all RC spectra, the small negative signal at ∼1740 cm^{-1} is essentially not affected by $^1H/^2H$ exchange.

Q_B^-/Q_B Spectra of Pro-L209 → Phe Mutant RCs Reconstituted with Site-Specific ^{13}C-Labeled Ubiquinone. The Q_B^-/Q_B spectra of the Tyr-L209 and Phe-L209 mutants display important changes as compared to WT RCs (Figures 2 and 3). To discriminate between changes due to different responses of the protein upon semiquinone formation in native and mutant RCs or different interactions of the quinone in the mutants, bonding interactions of Q_B and Q_B^- with the protein in the Tyr-L209 (*47*) and Phe-L209 RCs were investigated by using specifically labeled quinones to reconstitute the Q_B site. Figure 4 displays the Q_B^-/Q_B spectra of Phe-L209 RCs reconstituted with unlabeled Q_3 (e), $^{13}C_1$-labeled Q_3 (d), and $^{13}C_4$-labeled Q_3 (c), respectively. In these spectra, the regions between 1750 and 1650 cm^{-1}, 1600 and 1500 cm^{-1}, and 1400 and 1200 cm^{-1} which are not affected by the binding of labeled quinone, correspond mostly to the absorption of protein and unlabeled quinone (methyl, methoxy, and isoprenoid chain) groups. However, distinct isotopic effects for $^{13}C_1$- and $^{13}C_4$-labeling occur in the 1600−1625 cm^{-1} range and between 1500 and 1400 cm^{-1}. All these effects are best visualized in the "double-difference" spectra (Figure 4a,b) calculated from the individual Q_B^-/Q_B spectra recorded with RCs reconstituted with isotopically labeled and unlabeled Q_3 (^{13}C-minus-^{12}C). In such double-difference spectra, isotope-sensitive vibrations from the quinone itself can be separated from those of the protein that are expected
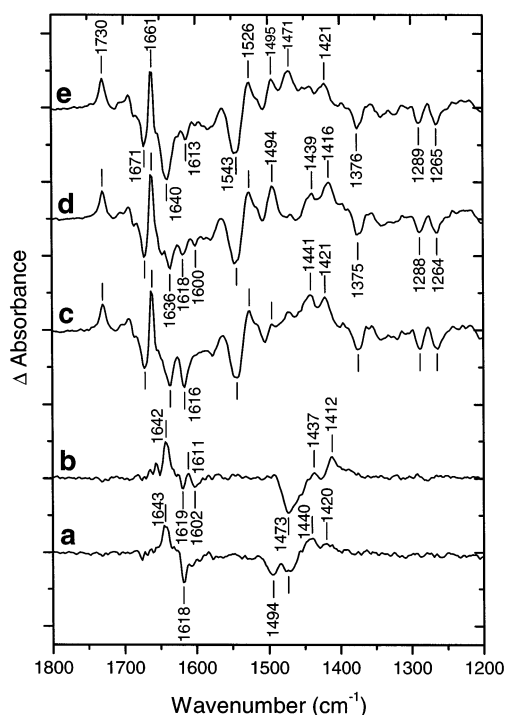
FIGURE 4: Light-induced Q_B^-/Q_B FTIR difference spectra at pH 7 and 15 °C of Pro-L209 → Phe mutant RCs reconstituted with (e) unlabeled Q_3, (d) $^{13}C_1$-labeled Q_3, and (c) $^{13}C_4$-labeled Q_3. Calculated double-difference spectra (isotopically labeled-minus-unlabeled) obtained for $^{13}C_1$-labeling (b), and $^{13}C_4$-labeling (a). About 150 000 interferograms were averaged. The tick marks on the vertical axis are separated by 10^{-4} absorbance unit.

Table 1: IR Frequencies (cm^{-1}) of the C=O and C=C Modes of Neutral Q_B in Wild-Type and Mutant RCs[a]

	C_1=O	C_4=O	C=C
Rb. sphaeroides	1641 (−21)	1641 (−23)	1610 (−10)
Pro-L209 → Phe	1642 (−23)	1643 (−25)	1611 (−9)
Pro-L209 → Tyr	1640 (−16)	1640 (−22)	1614 (−14)
Rp. viridis	1642 (−18)	1641 (−22)	1615 (−14)

[a] The frequency shifts of the C=O bands upon selective $^{13}C_1$- and $^{13}C_4$-labeling are indicated in brackets. The frequency shift of the C=C band is given for $^{13}C_1$-labeling while there is no observed shift for $^{13}C_4$-labeling. Data for *Rb. sphaeroides* and *Rp. viridis* RCs were taken from Breton et al. (*44*) and for the Tyr-L209 mutant from Breton et al. (*47*).

at 1437 and 1412 cm^{-1} for $^{13}C_1$-labeling, and at 1440 and 1420 cm^{-1} for $^{13}C_4$-labeling.

DISCUSSION

The present FTIR data show that several protein and semiquinone modes are severely affected upon first electron transfer to Q_B in *Rb. sphaeroides* mutant RCs in which Pro-L209 was replaced with Tyr, Phe, or Glu. These observations will be discussed in the frame of perturbations of the semiquinone−protein interactions and protein structural changes in these mutants. On the other hand, the overall similarity of the Q_B^-/Q_B spectra of WT and Thr-L209 RCs indicates strong structural analogies between the functional states Q_B and Q_B^- of the two RCs. Similar bonding interactions of the neutral secondary quinone with the protein found in all RCs will be related to an identical Q_B position in functional RCs.

Unique Q_B Binding Site in Mutant RCs at Position L209. The isotope-edited IR spectra of the Phe-L209 RCs reconstituted with selectively labeled Q_3 display a unique band at 1642−1643 cm^{-1} (Figure 4a,b). These data demonstrate that both C=O of neutral Q_B contribute equally at 1642−1643 cm^{-1} and that each carbonyl of Q_B is engaged in comparable interactions with the protein. The frequency downshift of the 1642−1643 cm^{-1} band with respect to isolated ubiquinone (1664−1650 cm^{-1}; *51, 52*) indicates moderate symmetrical hydrogen bonding of Q_B to the protein binding site. Table 1 shows that the C=O frequency of the Phe-L209 mutant is highly comparable to the one observed at 1641−1642 cm^{-1} for WT RCs from *Rb. sphaeroides* and *Rp. viridis* (*44*), and at 1640 cm^{-1} for the Tyr-L209 mutant (*47*). The 1−3 cm^{-1} frequency shift observed for the unique C=O band seen in all RCs (Table 1) could account for slight differences in hydrogen bond strengths or dielectric constant of the Q_B environment. In addition, the pattern and the frequencies of the C=C modes of Q_B in the Phe-L209 mutant show a shift of the positive band at 1611 to 1602 cm^{-1} upon $^{13}C_1$-labeling (Figure 4b), and no effect upon $^{13}C_4$-labeling (Figure 4a). A similar shift upon $^{13}C_1$-labeling has been observed in WT RCs from *Rb. sphaeroides* and *Rp. viridis*, as well as in Tyr-L209 RCs (Table 1). For isolated Q_3, the shift of the C=C mode is the same (from 1610 to 1600 cm^{-1}) for both $^{13}C_1$- and $^{13}C_4$-labeling indicating that the coupling of C=C and C=O modes at the C_1 and C_4 positions are equivalent (*44*). It therefore appears that in the Phe-L209 mutant, as previously reported for WT (*44*) and mutant (*46, 47*) RCs, the coupling of the C=C mode with the $^{13}C_1$=O mode is not identical to the one with the $^{13}C_4$=O mode. This means that the constraint of the protein in the environment of the C_1

to cancel.[3] The double-difference spectra $^{13}C_1$-minus-^{12}C and $^{13}C_4$-minus-^{12}C are displayed in Figure 4, panels b and a, respectively. In these spectra, the IR bands of the neutral unlabeled quinone (1660−1600 cm^{-1}) appear with a positive sign, while the downshifted bands of the labeled quinone exhibit a negative sign. The semiquinone bands in the 1500−1400 cm^{-1} range exhibit a reverse behavior. Such isotope-edited double-difference spectra for $^{13}C_1$- and $^{13}C_4$-labeling represent IR fingerprints for the interactions of the quinone and semiquinone in their respective protein binding site (*44, 47, 51*).

Both double-difference spectra of the Phe-L209 mutant (Figure 4a,b) show a main positive band at 1642−1643 cm^{-1} which is downshifted to 1619−1618 cm^{-1} upon $^{13}C_1$- or $^{13}C_4$-labeling. The 1642−1643 cm^{-1} band is attributed to each of the two C=O vibrations of the unlabeled Q_B in Phe-L209 RCs. While the two carbonyls of neutral Q_B absorb at the same frequency, an inequivalence of the C=C modes involving the C_1 and C_4 atoms is deduced from the observation of a differential signal at 1611/1602 cm^{-1} upon $^{13}C_1$-labeling (Figure 4b) while no such signal is present upon $^{13}C_4$-labeling (Figure 4a). In the semiquinone absorption range, the pattern of the bands shows one main negative band at 1473 cm^{-1} for $^{13}C_1$-labeling (Figure 4b), and two negative bands at 1494 and 1473 cm^{-1} for $^{13}C_4$-labeling (Figure 4a). For the labeled semiquinone, two positive bands are observed

---

[3] In spectra a and b of Figure 4, the cancellation of the bands in the 1655−1665 cm^{-1} range is not complete, leading to small signals attributed to residual protein (amide I) modes. Such features are also visible in double-difference spectra reported in Breton et al. (*44, 47*).

and C_4 atoms is not equivalent, so that the C_4 atom of Q_B is specifically perturbed compared to the isolated Q_3 molecule in solution. Possible explanations, involving the anchoring of the methyl group at C_5 and/or differences in the conformation of the two methoxy groups at C_2 and C_3, have been discussed in detail in a previous paper (*44*).

From the highly comparable IR fingerprints observed for the C=O and C=C modes of Q_B in WT and Tyr-L209 RCs, it has been previously concluded that the neutral state of the functional Q_B occupies the same binding site in these two RCs (*47*). The equivalence of frequency of the two carbonyls of Q_B rather favors the proximal Q_B binding site owing to its hydrogen bonding pattern described in the various X-ray structures of native and mutant RCs. In the proximal site, both C=O of Q_B are within hydrogen bonding distance to the surrounding protein (*25−30*), while in the distal site, only one C=O is described to interact with the protein (*2, 4, 30*). For the Tyr-L209 mutant, the FTIR data (*47*) fit the unique proximal Q_B site described for the location of the quinone in the dark-adapted structure at 5 °C of the crystals of this mutant RC (*25*). For WT RCs, our FTIR data also favored the proximal Q_B conformation as the binding site of neutral Q_B in functional RCs from *Rb. sphaeroides* and *Rp. viridis* (*47*). More generally, only one Q_B site is detected by FTIR spectroscopy in all native and mutant RCs (*44, 46, 47*). This is difficult to reconcile with the main distal Q_B structure found by Stowell et al. (*4*), in dark-adapted crystals of *Rb. sphaeroides* RCs as well as with the most recent X-ray structure of native RCs crystals from *Rb. sphaeroides* obtained by Fritszch et al. (*30*) showing heterogeneous bonding of the quinone with 55% Q_B occupying the distal site in the dark state. In contrast, it should be noticed that the FTIR data on *Rp. viridis* RCs (*44*) agree with the structurally best described Q_B site in *Rp. viridis* RCs (at 2.45 Å) showing a well-defined proximal position with full occupancy of the Q_B site (*32*).

Since the frequency of the two carbonyls and the IR fingerprint of the coupling of the C=O and C=C modes of Q_B in the Phe-L209 mutant are essentially the same as those described for native and Tyr-L209 RCs (Table 1), we propose that the neutral state of the functional Q_B in the Phe-L209 mutant also occupies the proximal site. A preliminary FTIR study of Glu-L209 RCs reconstituted with specifically ^{13}C-labeled quinones also suggests a unique proximal Q_B site (unpublished). At first sight, these FTIR conclusions are not in agreement with the X-ray structure analyses of the Phe-L209 and Glu-L209 RCs favoring an intermediate and distal position of Q_B, respectively. However, identification of the exact Q_B location in the structural models of these two mutant RCs was somewhat ambiguous (*25*).

Semiquinone (Q_B^-) Binding in Pro-L209 → Tyr and Pro-L209 → Phe Mutants: Comparison with Native RCs. The Q_B^-/Q_B spectra of the Tyr-L209 and Phe-L209 mutant RCs are closely related in the semiquinone absorption range (Figure 2e,d). However, they display large changes with respect to the spectrum of *Rb. sphaeroides* RCs (Figure 2a), suggesting different interactions of Q_B^- with the protein in these mutants as compared to WT RCs. In WT RCs from *Rb. sphaeroides*, the main anion band at 1479 cm^{-1} (Figure 2a, Table 2) is similarly shifted by either ^{13}C$_1$ and ^{13}C$_4$ labels (*44*). Consequently, the 1479 cm^{-1} band has been previously

Table 2: IR Frequencies (cm^{-1}) of the Semiquinone Q_B^- Modes in Wild-Type and Mutant RCs Observed in the ^{13}C$_1$-minus-^{12}C (first column) and ^{13}C$_4$-minus-^{12}C (second column) Double-Difference Spectra[a]

	^{13}C$_1$-minus-^{12}C	^{13}C$_4$-minus-^{12}C
Rb. sphaeroides	1479 (−)	1479 (−)
	1489 (+), 1461 (−)	1491 (−), 1461 (−)
Pro-L209 → Phe	1473 (−)	1494 (−), 1473 (−)
Pro-L209 → Tyr	1473 (−)	1494 (−), 1470 (−)
Rp. viridis	1475 (−)	1475 (−)
	1489 (+), 1461 (−)	1490 (−), 1466 (−)

[a] (+) and (−) indicate positive and negative peaks, respectively, in the double-difference spectra. Data for *Rb. sphaeroides* and *Rp. viridis* RCs were taken from Breton et al. (*44*) and for the Tyr-L209 mutant from Breton et al. (*47*).

attributed to the two C⋯O modes coupled to C⋯C modes of the semiquinone. Small shoulders at ∼1490 and 1461 cm^{-1} (Table 2) on the main 1479 cm^{-1} peak have been tentatively assigned to C⋯C modes (*44*). Moreover, the ∼1490 cm^{-1} shoulder exhibits different behaviors upon selective ^{13}C$_1$- or ^{13}C$_4$-labeling, leading to the observation of a positive signal at 1489 cm^{-1} in the ^{13}C$_1$-minus-^{12}C double difference spectrum of WT RCs and a negative signal at 1491 cm^{-1} in the ^{13}C$_4$-minus-^{12}C spectrum. This reveals an inequivalence of the C⋯C modes of the semiquinone involving the C_1 and C_4 atoms, as also observed for the C=C modes of neutral Q_B (*44*). Nevertheless, the absence of splitting of the 1479 cm^{-1} band and its comparable frequency downshift upon either ^{13}C$_1$- or ^{13}C$_4$-labeling favor equivalent hydrogen bonding interactions of the two carbonyls of Q_B^- to the protein in WT RCs. In *Rp. viridis* RCs (Table 2), the main anion band peaks at 1475 cm^{-1} with shoulders at 1493 and 1461 cm^{-1} which have been also tentatively assigned to C⋯C modes (*44*). Here also, the pattern of the highest frequency feature leads to positive (at 1489 cm^{-1}) and negative (at 1490 cm^{-1}) signals in the ^{13}C$_1$-minus-^{12}C and ^{13}C$_4$-minus-^{12}C double-difference spectra, respectively.

The double-difference spectra (^{13}C$_1$-minus-^{12}C and ^{13}C$_4$-minus-^{12}C) of the two aromatic mutants show a clear inequivalence of the modes involving the C_1 and C_4 atoms with one main negative band at 1473 cm^{-1} upon ^{13}C$_1$-labeling and two negative bands of comparable amplitude at 1494 and 1473−1470 cm^{-1} upon ^{13}C$_4$-labeling (Figure 4a,b; Table 2). In both Tyr-L209 and Phe-L209 RCs, the observations of two bands at 1494 and 1473−1470 cm^{-1} upon ^{13}C$_4$-labeling, together with the absence of any peak at 1494 cm^{-1} upon ^{13}C$_1$-labeling point to an assignment of the 1494 cm^{-1} signal to a semiquinone mode which predominantly involves motion of the C_4-atom. Contributions from both ^{13}C$_1$ and ^{13}C$_4$ modes occur at 1473−1470 cm^{-1}. Further studies of L209 mutant RCs reconstituted with quinone labeled with ^{18}O on both carbonyls would be necessary to investigate the relative contribution of the C⋯O and C⋯C modes at 1494 and 1473−1470 cm^{-1}.

Interestingly, the IR fingerprint spectra (^{13}C$_1$-minus-^{12}C and ^{13}C$_4$-minus-^{12}C) of the aromatic mutants (Figure 4a,b; *47*) are much closer to those for *Rp. viridis* than for *Rb. sphaeroides* (Table 2; *44*), i.e., similarities in the pattern and the relative amplitudes of the positive and negative bands are observed in the semiquinone range of the double-difference spectra of Tyr-L209, Phe-L209, and *Rp. viridis*

RCs. Notably, for the labeled semiquinone, the amplitude of a mode at 1412 cm^{-1} is found to be larger for labeling at the 1- than at the 4-position while the situation is reversed for a mode at around 1440 cm^{-1} (Figure 4a,b; *47*), as also observed for WT RCs from *Rp. viridis*, and to a lesser extent for WT RCs from *Rb. sphaeroides* (*44*). The larger width and the 4 cm^{-1} downshift of the main anion band in *Rp. viridis* (1475 cm^{-1}) compared to *Rb. sphaeroides* (1479 cm^{-1}) has been previously related to the few residues lining the Q_B pocket that differ between the two organisms (*44*) and that can differently affect the electrostatic environment of the quinone.

In the aromatic mutants, the introduction of a Tyr or Phe at position L209 induces a displacement of several polar side chains (*25*), some of them belonging to the carboxylic cluster near Q_B. Therefore, the charge distribution near the cluster should be different in the aromatic mutants compared to WT RCs, and consequently, it could have an effect on the coupling of the C$\cdots$O and C$\cdots$C modes of the Q_B^- anion, and thus on the frequency/intensity of the semiquinone bands in the spectra of the mutant RCs. Alternatively, a change in the electrostatic around the secondary quinone in the aromatic mutants could induce a minor displacement of the semiquinone ring compared to the position of the Q_B^- ring in WT RCs. It is generally admitted that the semiquinone in native and mutant RCs occupies an identical (proximal) position. The differences observed between the IR fingerprints of the semiquinone in WT RCs from *Rb. sphaeroides* and *Rp. viridis* and in the two aromatic mutant RCs are probably not related to a different site of Q_B^- in the mutants with respect to WT RCs and can be explained by a different coupling of the C$\cdots$O and C$\cdots$C modes in the anion of the mutants. However, a small displacement of the semiquinone ring within the proximal site in the aromatic mutants cannot be totally excluded from the present IR data.

IR Response of the Protein upon Q_B Reduction in the L209 Mutant RCs. (a) Absence of Additional Structural Changes in the Thr-L209 Mutant Compared to Native RCs. The overall similarity of the Q_B^-/Q_B spectra of WT and Thr-L209 RCs either in ^1H_2O or ^2H_2O, notably in the quinone/semiquinone and amide I (at 1652/1641 cm^{-1}) regions, indicates large structural analogies between the functional states Q_B and Q_B^- of the two RCs. In agreement with these FTIR data, comparable kinetic and energetic parameters were observed for the first and second electron-transfer steps in these two RCs (*23*).

(b) Structural Changes Observed in the Glu-L209 RCs upon Q_B^- Formation. With respect to WT RCs, the Q_B^-/Q_B spectrum of Glu-L209 RCs shows several differences, i.e., in the amide I (at 1652 and 1661 cm^{-1}) and amide II (at 1548 and 1527 cm^{-1}) regions as well as in the semiquinone absorption range where the shoulder at 1495 cm^{-1} on the main anion peak at 1476 cm^{-1} is more pronounced than the one at ~1491 cm^{-1} on the 1479 cm^{-1} peak of WT RCs. All these observations are indicative of different structural changes accompanying Q_B reduction in this mutant as compared to WT RCs. It has to be noticed that protein structural changes and perturbations of the semiquinone−protein interactions are smaller in the Glu-L209 RCs than in the aromatic mutants (see next section). These FTIR results are in agreement with the X-ray structural models of the Tyr-L209 (Figure 1) and Phe-L209 RCs showing local structural changes in the aromatic mutants and no significant structural changes in the Glu-L209 RC, except for the introduced carboxylic side chain of Glu-L209 located within the water chain (*25*).

(c) Similar Structural Changes Induced by the Tyr-L209 and Phe-L209 Mutations upon Q_B^- Formation. It is worth noting that the overall shape of the Q_B^-/Q_B spectra of the two aromatic mutants is strikingly comparable both in ^1H_2O (Figure 2d,e) and ^2H_2O (Figure 3d,e). More specifically, the Q_B^-/Q_B spectra of the two aromatic mutants are very comparable in the absorption range of amide I/side chain (at 1666−1670 cm^{-1} and 1661−1651/1638−1639 cm^{-1}) and amide II (at 1548−1543/1528−1527 cm^{-1}) modes. It can thus be concluded that the introduction of a Tyr or a Phe side chain at the L209 position leads to similar protein rearrangements (backbone and side chains) upon first electron transfer to Q_B in these two mutant RCs. The large negative signal seen at 1666−1670 cm^{-1} in ^1H_2O (Figure 2d,e) and which is downshifted by 1−5 cm^{-1} in ^2H_2O (Figure 3d,e) in the spectra of Tyr-L209 and Phe-L209 RCs, could arise from a peptide C=O or a side chain mode. Several amino acid side chains (Asn, Gln, and Arg) could contribute to the 1670−1680 cm^{-1} spectral range (*53, 54*); however, the ^1H/^2H isotopic effect is expected to be larger than 1−5 cm^{-1} (*55*). The 1666−1670 cm^{-1} band as well as the 1661−1651/1638−1639 cm^{-1} differential signal are more compatible with an assignment to a conformational change of peptide C=O group(s) upon Q_B^- formation.

Local structural changes near Q_B have been reported in the X-ray structures of the two mutants Tyr-L209 (Figure 1) and Phe-L209 (*25*). Notably, comparable displacements of the Asp-L213 (1.7 Å), Thr-L226 (2.6 Å), and Glu-H173 (1.2 Å) side chains occur (Figure 1) in the two aromatic mutants, and a hydrogen bond not seen in WT RCs is formed between Glu-H173 and Arg-H177. In the Q_B^-/Q_B spectra of Tyr-L209 and Phe-L209 RCs, the signals observed in the 1670−1650 cm^{-1} range might arise from a small perturbation delocalized over several different residues such as the ones described above, or a localized perturbation at a specific amino acid. Another possibility would be a localized conformational change at the site of the mutation. In this latter case, the large differential signal observed in the amide II region at ~1548/1527 cm^{-1} of the Tyr-, Phe-, and Glu-L209 RCs support a conformational change of the peptide NH at position L209 upon replacement of an imino acid (Pro) with an amino (Tyr, Phe, Glu) acid. Considering both the X-ray (*25*) and FTIR data on the Tyr-L209 and Phe-L209 RCs, it can be concluded that the introduction of Tyr or Phe at the position L209 causes similar rearrangement of the organized pattern near Q_B, and that this pattern is similarly affected by Q_B reduction in the two aromatic mutants.

(d) Contribution of Protonated Carboxylic Acids. In native RCs, protonation of Glu-L212 upon formation of Q_B^- is characterized by an absorption increase at 1728 cm^{-1} in ^1H_2O (1718 cm^{-1} in ^2H_2O) and is found to proceed with the same kinetics as reduction of Q_B (*14, 15*). FTIR spectroscopy combined with site-directed mutagenesis has revealed that Glu-L212 is the main contributor of the carboxylic cluster nearby Q_B to proton uptake (0.3−0.4 H$^+$/Q_B^-/Glu-L212 at pH 7; *14*) upon reduction of Q_B in *Rb. sphaeroides* RCs (*14, 19−21*).

The Thr-L209 and Glu-L209 RCs show comparable features with respect to WT RCs, i.e., a main peak at $1728-1729$ cm^{-1} in ^1H_2O (Figure 2), a new feature at 1718 cm^{-1} in ^2H_2O with a remaining signal at $1729-1730$ cm^{-1} (Figure 3). This comparable behavior of the main carboxylic band in the Thr-L209 and Glu-L209 mutant RCs as well as in native RCs strongly favors the involvement of a common residue. The positive signal at $1728-1729$ cm^{-1} in the Q_B^-/Q_B spectra of Glu-L209 and Thr-L209 RCs is thus attributed to a (partial) protonation of Glu-L212 upon reduction of Q_B. In the X-ray structure of the Glu-L209 mutant RC (*25*), the introduced Glu-L209 side chain replaces two water molecules and the formation of a hydrogen bond between Glu-L212 and Glu-L209 is proposed, suggesting that one of these residues (Glu-L212) is protonated. The present FTIR data suggest that, in the Glu-L209 mutant, Glu-L212 is at least partially ionized in the Q_B neutral state, and thus Glu-L209 would have to be at least partially protonated.

In the absorption range of protonated carboxylic groups, the main peak of the Q_B^-/Q_B spectra of Tyr-L209 and Phe-L209 RCs in ^1H_2O is upshifted by 3 and 2 cm^{-1}, respectively, compared to the 1728 cm^{-1} peak in WT RCs (Figure 2). The corresponding spectra in ^2H_2O show a positive signal at $1731-1732$ cm^{-1} with no apparent new feature at lower frequency, as it is observed at 1718 cm^{-1} for WT, Glu-L209, and Thr-L209 RCs (Figure 3). Perturbation of the Glu-L212 environment in the aromatic mutants might account for such effects. However, an unambiguous attribution of the $1731-1730$ cm^{-1} signals in the Tyr-L209 and Phe-L209 RCs would deserve further investigation.

CONCLUSION

The structural properties of the Thr-L209 mutant RCs monitored by light-induced FTIR difference spectroscopy of the reduction of the secondary quinone are essentially the same as those for WT RCs, in agreement with similar functional characteristics of WT and Thr-L209 RCs (*23*). For the Tyr-L209, Phe-L209, and Glu-209 mutant RCs, the reduction of Q_B is accompanied by protein rearrangements (backbone and/or side chains) with similar structural changes occurring in the two aromatic mutants while smaller changes are observed in the Glu-L209 RC.

The isotope-edited IR fingerprints for the semiquinone Q_B^- of the Tyr-L209 and Phe-L209 mutant RCs display changes as compared to WT RCs, indicative of different interactions of the quinone anion with the protein in these mutants. In contrast, the IR fingerprints for the neutral Q_B binding site of native and mutant (Tyr-, Phe-, and Glu-L209) RCs all show a unique C=O band at $1643-1640$ cm^{-1} and a similar inequivalence of the C=C modes for selective labeling at C_1 or at C_4. The $1643-1640$ cm^{-1} frequency is indicative of moderate and symmetrical hydrogen bonding of the two C=O of neutral Q_B with the protein binding site. It is concluded that in all RCs the functional state of the neutral Q_B occupies a unique binding site which is favored to be the position proximal to the non-heme iron.

REFERENCES

1. Okamura, M. Y., Paddock, M. L., Graige, M. S., and Feher, G. (2000) *Biochim. Biophys. Acta 1458*, 148−163.
2. Ermler, U., Fritzsch, G., Buchanan, S. K., and Michel, H. (1994) *Structure 2*, 925−936.
3. Lancaster, C. R. D., Ermler, U., and Michel, H. (1995) in *Anoxygenic Photosynthetic Bacteria* (R. E. Blankenship, M. T. Madigan, and C. E. Bauer, Eds.) pp 503−526, Kluwer Academic Publishers, The Netherlands.
4. Stowell, M. H. B., McPhillips, T. M., Rees, D. C., Soltis, S. M., Abresch, E., and Feher, G. (1997) *Science 276*, 812−816.
5. Fritzsch, G., Kampmann, L., Kapaun, G., and Michel, H. (1998) *Photosynth. Res. 55*, 1−6.
6. Abresch, E. C., Paddock, M. L., Stowell, M. H. B., McPhillips, T. M., Axelrod, H. L., Soltis, S. M., Rees, D. C., Okamura, M. Y., and Feher, G. (1998) *Photosynth. Res. 55*, 119−125.
7. Shinkarev, V. P. and Wraight, C. A. (1993) in *The Photosynthetic Reaction Center* (J. Deisenhofer, J. R. Norris, Eds) pp 193−255, Academic Press, New York.
8. Sebban, P., Maróti, P., and Hanson, D. H. (1995) *Biochimie 77*, 677−694.
9. Paddock, M. L., Graige, M. S., Feher, G., and Okamura, M. Y. (1999) *Proc. Natl. Acad. Sci. U.S.A. 96*, 6183−6188.
10. Paddock, M. L., Feher, G., and Okamura, M. Y. (2000) *Proc. Natl. Acad. Sci. U.S.A. 97*, 1548−1553.
11. Ädelroth, P., Paddock, M. L., Tehrani, A., Beatty, J. T., Feher, G., and Okamura, M. Y. (2001) *Biochemistry 40*, 14538−14546.
12. Gerencsér, L., and Maróti, P. (2001) *Biochemistry 40*, 1850−1860.
13. Gerencsér, L., Taly, A., Baciou, L., Maróti, P., and Sebban, P. (2002) *Biochemistry 41*, 9131−9138.
14. Nabedryk, E., Breton, J., Hienerwadel, R., Fogel, C., Mäntele, W., Paddock, M. L., and Okamura, M. Y. (1995) *Biochemistry 34*, 14722−14732.
15. Hienerwadel, R., Grzybek, S., Fogel, C., Kreutz, W., Okamura, M., Y., Paddock, M. L., Breton, J., Nabedryk, E., and Mäntele, W. (1995) *Biochemistry 34*, 2832−2843.
16. Ädelroth, P., Paddock, M. L., Sagle, L. B., Feher, G., and Okamura, M. Y. (2000) *Proc. Natl. Acad. Sci. U.S.A. 97*, 13086−13091.
17. Paddock, M. L., Ädelroth, P., Feher, G., Okamura, M. Y., and Beatty, J. T. (2002) *Biochemistry 41*, 14716−14725.
18. Mezzetti, A., Nabedryk, E., Breton, J., Okamura, M., Y., and Paddock, M., L., Giacometti, G., and Leibl, W. (2002) *Biochim. Biophys. Acta 1453*, 320−330.
19. Nabedryk, E., Breton, J., Okamura, M., Y., and Paddock, M. L. (1998) *Biochemistry 37*, 14457−14462.
20. Nabedryk, E., Breton, J., Joshi, H. M., and Hanson, D. K. (2000) *Biochemistry 39*, 14654−14663.
21. Nabedryk, E., Breton, J., Okamura, M. Y., and Paddock, M. L. (2001) *Biochemistry 40*, 13826−13832.
22. Baciou, L., and Michel, H. (1995) *Biochemistry 34*, 7967−7972.
23. Tandori, J., Sebban, P., Michel, H., and Baciou, L. (1999) *Biochemistry 38*, 13179−13187.
24. Tandori, J., Maroti, P., Alexov, E., Sebban, P., and Baciou, L. (2002) *Proc. Natl. Acad. Sci. U.S.A. 99*, 6702−6706.
25. Kuglstatter, A., Ermler, U., Michel, H., Baciou, L., and Fritzsch, G. (2001) *Biochemistry 40*, 4253−4260.
26. Allen, J. P., Feher, G., Yeates, T. O., Komiya, H., and Rees, D. C. (1988) *Proc. Natl. Acad. Sci. U.S.A. 85*, 8487−8491.
27. El-Kabbani, O., Chang, C.-H., Tiede, D., Norris, J., and Schiffer, M. (1991) *Biochemistry 30*, 5361−5369.
28. Chirino, A. J., Lous, E. J., Huber, M., Allen, J. P., Schenck, C. C., Paddock, M. L., Feher, G., and Rees, D. C. (1994) *Biochemistry 33*, 4584−4593.
29. Arnoux, B., and Reiss-Husson, F. (1996) *Eur. Biophys. J. 24*, 233−242.
30. Fritzsch, G., Koepke, J., Diem, R., Kuglstatter, A. and Baciou, L. (2002) *Acta Crystallogr. D58*, 1660−1663.
31. Graige, M. S., Feher, G., and Okamura, M. Y. (1998) *Proc. Natl. Acad. Sci. U.S.A. 95*, 11679−11684.
32. Lancaster, C. R. D., and Michel, H. (1997) *Structure 5*, 1339−1359.
33. Rabenstein, B., Ullmann, G. M., and Knapp E.-W. (2000) *Biochemistry 39*, 10487−10496.
34. Grafton, A. K., and Wheeler, R. A. (1999) *J. Phys. Chem. B 103*, 5380−5387.
35. Walden, S. E., and Wheeler, R. A. (2002) *J. Phys. Chem. B 106*, 3001−3006.

36. Cherepanov, D. A., Bibikov, S. I., Bibikova, M. V., Bloch, D. A., Drachev, L. A., Gopta, O. A., Oesterhelt, D., Semenov, A. Y., Mulkidjanian, A. Y. (2000) *Biochim. Biophys. Acta 1459*, 10−34.

37. Zachariae, U., and Lancaster, C. R. D., (2001) *Biochim. Biophys. Acta 1505*, 280−290.

38. Taly, A., Sebban, P., Smith, J. C., and Ullmann, G. M. (2003) *Biophys J. 84*, 2090−2098.

39. Li, J., Gilroy, D., Tiede, D. M., and Gunner, M. R. (1998) *Biochemistry 37*, 2818−2829.

40. Xu, Q., and Gunner, M. R. (2002) *Biochemistry 41*, 2694−2701.

41. Xu, Q., Baciou, L., Sebban, P., and Gunner, M. R. (2002) *Biochemistry 41*, 10021−10025.

42. Breton, J., and Nabedryk, E. (1996) *Biochim. Biophys. Acta 1275*, 84−90.

43. Breton, J., Berthomieu, C., Thibodeau, D. L., and Nabedryk, E. (1991) *FEBS Lett. 288*, 109−113.

44. Breton, J., Boullais, C., Berger, G., Mioskowski, C., and Nabedryk, E. (1995) *Biochemistry 34*, 11606−11616.

45. Brudler, R., de Groot, H. J. M., van Liemt, W. B. S., Gast, P., Hoff, A. J., Lugtenburg, J., and Gerwert, K. (1995) *FEBS Lett. 370*, 88−92.

46. Breton, J., Nabedryk, E., Boullais, C., Mioskowski, C., Paddock, M. L., Feher, G., and Okamura, M. Y. (1997) *Biophys. J. 72*, A7.

47. Breton, J., Boullais, C., Mioskowski, C., Sebban, P., Baciou, L., Nabedryk, E. (2002) *Biochemistry 41*, 12921−12927.

48. Boullais, C., Nabedryk, E., Burie, J.-R., Nonella, M., Mioskowski, C., and Breton, J. (1998) *Photosynth. Res. 55*, 247−252.

49. Krimm, S., and Bandekar, J. (1986) *Adv. Protein Chem. 38*, 181−364.

50. Breton, J., Nabedryk, E., Allen, J. P., and Williams, J. C. (1997) *Biochemistry 36*, 4515−4525.

51. Breton, J., Boullais, C., Burie, J.-R., Nabedryk, E., and Mioskowski, C., (1994) *Biochemistry 33*, 14378−14386.

52. Burie, J.-R., Boullais, C., Nonella, M., Mioskowski, C., Nabedryk, E., and Breton, J. (1997) *J. Phys. Chem. B 101*, 6607−6617.

53. Venyaminov, S. Yu., and Kalnin, N. N. (1990) *Biopolymers 30*, 1243−1257.

54. Rahmelov, K., Hübner, W., and Ackerman, Th. (1998) *Anal. Biochem. 257*, 1−11.

55. Chirgadze, Yu. N., Fedorov, O. V., and Trushina, N. P. (1975) *Biopolymers 14*, 679−694.